# Dynamic Load Balancing with Handover in Hybrid Li-Fi and Wi-Fi Networks

# Dynamic Load Balancing with Handover in Hybrid Li-Fi and Wi-Fi Networks

Yunlu Wang and Harald Haas

***Abstract*—In this paper, a hybrid network combining light fidelity (Li-Fi) with a radio frequency (RF) wireless fidelity (Wi-Fi) network is considered. An additional tier of very small Li-Fi attocells which utilise the visible light spectrum offers a significant increase in wireless data throughput in an indoor environment while at the same time providing room illumination. Importantly, there is no interference between Li-Fi and Wi-Fi. A Li-Fi attocell covers a significantly smaller area than a Wi-Fi access point (AP). This means that even with moderate user movement a large number of handover between Li-Fi attocells can occur, and this compromises the system throughput. Dynamic load balancing (LB) can mitigate this issue so that quasi-static users are served by Li-Fi attocells while moving users are served by a Wi-Fi AP. However, due to user movement, local overload situations may occur which prevent handover, leading to a lower throughput. This research studies LB in a hybrid Li-Fi/Wi-Fi network by taking into account user mobility and handover signalling overheads. Furthermore, a dynamic LB scheme is proposed, where the utility function considers system throughput and fairness. In order to better understand the handover effect on the LB, the service areas of different APs are studied, and the throughput of each AP by employing the proposed LB scheme is analysed.**

***Index Terms*—Li-Fi, Wi-Fi, Hybrid network, Load balancing, Handover overhead, VLC**

## I. Introduction

The increasing number of multi-media mobile devices and the extensive use of data-demanding mobile applications means that current mobile networks are at their maximum capacity due to the limited availability of the radio frequency (RF) spectrum. Li-Fi technology, which uses 300 THz licence-free and unused optical spectrum for wireless communications, has recently been regarded as a solution to this problem [1]. One advantage of Li-Fi is that it does not cause interference to existing RF communication systems, because it uses an entirely different part of the electromagnetic spectrum [2]. This enables the creation of hybrid networks that combine Li-Fi with RF systems.

In an indoor situation, a hybrid integration of Wi-Fi and Li-Fi is expected to improve both the system throughput and the user's quality of service (QoS) [3]. Since Li-Fi does not affect Wi-Fi coverage and throughput, the total system throughput of a Li-Fi/Wi-Fi hybrid network is always greater than that of separate Wi-Fi or Li-Fi networks [2]. On the one hand, according to the IEEE 802.11ad standard, the latest Wi-Fi protocol provided by Wireless Gigabit Alliance (WiGig) enables devices to operate in three centre frequencies (2.4, 5 and 60 GHz), and WiGig can achieve a total data rate up to 7 Gb/s [4]. On the other hand, recent research shows that the achievable data rate of a single LED can be more than 3 Gb/s [5]. A large number of Li-Fi APs can be deployed in an indoor scenario and thus a high area spectral efficiency can be achieved with a Li-Fi network [6], and the total throughput of a Li-Fi/Wi-Fi hybrid system can be considerable. Also, a hybrid network can improve the user QoS by ensuring a high throughput at all locations. In general, Wi-Fi can achieve ubiquitous coverage which provides the basic data rate requirement and Li-Fi can significantly augment the maximum capacity.

In a hybrid Li-Fi/Wi-Fi network, fair and efficient load balancing (LB) can be a challenge due to the small size of Li-Fi attocells. Most of the recent research focuses on the resource allocation (RA) problem in static systems where users are assumed to be fixed [2], [7]. However, in practical scenarios, some users will be moving. In an indoor scenario, the coverage of a Wi-Fi AP is beyond a single room whereas each Li-Fi cell in a Li-Fi network covers only a few square meters due to the rectilinear propagation of light. However, there are many light sources in a room for illumination purposes and Li-Fi harnesses significant gains by reusing transmission resources. As a consequence, when assuming user movement, users may experience many handovers between Li-Fi attocells. The handover between Li-Fi attocells is termed as horizontal handover, and the handover between Li-Fi and Wi-Fi APs is termed as vertical handover. During a handover, the signalling information is exchanged between users and a central unit (CU). This process takes an average time varying from around 30 ms to 3000 ms depending on the algorithms used [8], [9] and transmission losses occur in this period. Thus, the handover overhead must be considered in the design of LB schemes for such hybrid networks. In conventional mobile RF networks, handover occurs when users receive a lower signal-to-noise ratio (SNR) from the serving base station (BS) than that from other BSs [10]. However, in an indoor hybrid network, the stability issues have to be taken into account as a handover may prompt further handovers. For example, if a user is transferred from the Li-Fi layer to the Wi-Fi layer, it will increase the load in the respective Wi-Fi cell. Other users served by this Wi-Fi AP may have to be transferred to neighbouring Wi-Fi APs, or have reduced data rates. Also, due to the decrease in the load of the Li-Fi attocell, resources are freed up to enhance data rates to existing users. Thus, the aim is to develop LB schemes that ensure high user throughput,

The authors are with the University of Edinburgh, Li-Fi R&D Centre, Edinburgh, EH9 3JL, UK, (e–mail: {yunlu.wang, h.haas}@ed.ac.uk.) This publication acknowledges support from the Engineering and Physical Sciences Research Council (EPSRC) under Established Career Fellowship grant EP/K008757/1.

reduced handover overhead, fairness and stability in a hybrid Li-Fi/Wi-Fi system.

The rest of the paper is organised as follows: The hybrid system model with mobile devices is introduced in Section II. A detailed description of the proposed dynamic LB scheme is given in Section III. The throughput analysis is carried out in Section IV. The performance evaluation is presented and discussed in Section V. Conclusions are given in Section VI.

## II. System Model

### A. System setup

As shown in Fig. 1, a Li-Fi/Wi-Fi hybrid downlink system model is considered. This hybrid network covers an indoor area by $N_c$ Li-Fi APs and a single Wi-Fi AP. In the scenario, users are uniformly distributed and move randomly. All of the APs are connected to a CU through error free inter-connection links. Each Li-Fi AP is a large light emitting diode (LED) lamp which contains many low power LEDs, and each user has a photo detector (PD). It is assumed that all of the PDs are oriented perpendicular to the floor. This means that the angle of irradiation is equal to the angle of incidence. The field of view (FoV) of the LEDs and PDs can be designed so that the transmission can be contained within a certain space. Also, the walls of a room block light completely which means that there is no co-channel interference between rooms. Thus, each Li-Fi AP in this model covers a confined area, regarded as an attocell. In each attocell, the Li-Fi APs use the same modulation bandwidth. Users that reside in the overlapping area of Li-Fi attocells and are served by the Li-Fi APs would experience co-channel interference (CCI), which is treated as additional noise in this study. The Wi-Fi AP is assumed to cover the entire indoor area. Each user is either connected to a Li-Fi AP or the Wi-Fi AP for downlink wireless communications.

In this hybrid network, due to the fluctuating channel state information (CSI) of mobile users, the network load balancing should be undertaken in regular intervals. It is assumed that the CSI in both Li-Fi and RF systems remains constant for a short period which is defined as a state, and changes to a new value in the next state. The interval time between two neighbouring states is denoted by $T_p$. In each state, the load balancing configuration is assumed to be fixed and users receive constant data rates. The natural number $n$ denotes the sequence number of the states.

In the model, $\mathcal{C} = \{c|\ c \in [0, N_c], c \in \mathbb{Z}\}$ is denoted as the set of Li-Fi APs and the Wi-Fi AP, where $c = 0$ represents the Wi-Fi AP and $1 \leq c \leq N_c$ represents the Li-Fi APs. The set of users is denoted by $\mathcal{U}$. A full buffer traffic model is considered so that the maximum achievable data rate can be evaluated for each user at all times.

### B. Li-Fi channel model

The optical channel gain in indoor scenarios consists of the line of sight (LoS) component and the reflection component.

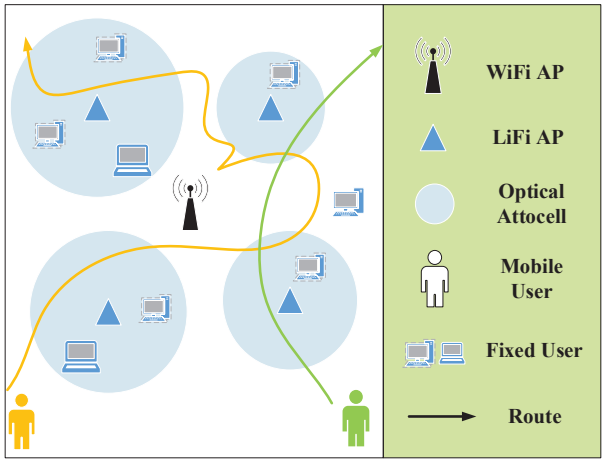


Fig. 1. System model

The LoS channel gain is expressed as [11]:

$$H_{\mu,\alpha} = \begin{cases} \frac{(m+1)A_p}{2\pi(z_{\mu,\alpha}^2+h^2)} g(\theta) T_s(\theta) \cos^m(\phi)\cos(\theta), & \theta < \Theta_F \\ 0, & \theta < \Theta_F \end{cases}, \tag{1}$$

where $m$ is the Lambertian index which is a function of the half-intensity radiation angle $\theta_{1/2}$, expressed as $m = -1/\log_2(\cos(\theta_{1/2}))$; $A_p$ is the physical area of the receiver photo-diode; $z_{\mu,\alpha}$ is the horizontal distance between Li-Fi AP $\alpha$ to user $\mu$; $h$ is the height of the room; $\phi$ is the angle of irradiation; $\theta$ is the angle of incidence; $\Theta_F$ is the half angle of the receiver's FoV; $T_s(\theta)$ is the gain of the optical filter; and $g(\theta)$ is the concentrator gain, which can be written as:

$$g(\theta) = \begin{cases} \frac{\chi^2}{\sin^2 \Theta_F}, & 0 \leq \theta \leq \Theta_F \\ 0, & \theta > \Theta_F \end{cases}, \tag{2}$$

where $\chi$ is the refractive index. According to [12], the reflection component is negligible when the Li-Fi baseband modulation bandwidth $B$ is less than 25 MHz. In this study, it is assumed that $B = 20$ MHz and the reflection component is not considered in the Li-Fi channel model.

In Li-Fi systems, the baseband communication with intensity modulation (IM) and direct detection (DD) is used [13]. The Li-Fi signals are transmitted in the form of optical power, which should be positive and real. In this study, the direct current biased optical orthogonal frequency division multiplexing (DCO-OFDM) method is employed [13]. The DC optical power is denoted by $P_{\text{opt}}$, and the DC bias added to the modulated signals ensures the output signals are positive. Moreover, in order to guarantee the real-valued signals, all of the symbols on OFDM subcarriers are designed to be Hermitian symmetric, and thus the signals transmitted in the time domain are converted to real numbers. In this case, only half of the bandwidth is used for data transmission. In addition, the LED lamps would operate in the linear region where the output optical power is proportional to the modulated input voltage. This region henceforth is termed as the linear working region of the LED. The signals outside this region

TABLE I
WI-FI THROUGHPUT

| Protocol Name | Carrier Frequency (GHz) | Bandwidth (MHz) | Spatial Stream | Throughput |
|---|---|---|---|---|
| 802.11 n | 2.4 | 20 | 1 | 120 Mb/s |
| 802.11 n | 5 | 40 | 1 | 600 Mb/s |
| 802.11 ac | 5 | 80 | 4 | 1 Gb/s |
| 802.11 ac | 5 | 160 | 4 | 2.4 Gb/s |
| 802.11 ac | 5 | 160 | 8 | 6.7 Gb/s |

are clipped before transmission. The conversion between the average electric power of signals and the average optical power obeys the following relationship [13]:

$$\iota = P_{\text{opt}}/\sqrt{P_{\text{elec}}}, \tag{3}$$

where $P_{\text{elec}}$ is the electric power of the signals. An increase of $\iota$ results in a decrease of the probability of the Li-Fi signals being outside the LED linear working region. In general, $\iota = 3$ can guarantee that less than 1% of the signals are clipped. In this case, the clipping noise can be considered negligible.

The signal-to-interference-plus-noise ratio (SINR) for user $\mu$ and AP $\alpha$ can be written as:

$$\text{SINR}_{\mu,\alpha} = \frac{(\kappa P_{\text{opt}} H_{\mu,\alpha})^2}{\iota^2 N_0 B + \sum (\kappa P_{\text{opt}} H_{\mu,\text{else}})^2}, \tag{4}$$

where $\kappa$ is the optical to electric conversion efficiency at the receivers; $N_0$ [A$^2$/Hz] is the noise power spectral density; $H_{\mu,\alpha}$ is the channel gain between user $\mu$ and Li-Fi AP; and $H_{\mu,\text{else}}$ is the channel gain between user $\mu$ and the interfering Li-Fi APs, according to (1). Shannon capacity is used for calculating the achievable data rate between user $\mu$ and Li-Fi AP $\alpha$. Since only half of the bandwidth can be used for data transmission in DCO-OFDM system, the achievable data rate is expressed as:

$$R_{\mu,\alpha}^{(n)} = B \log_2(1 + \text{SINR}_{\mu,\alpha}^{(n)}). \tag{5}$$

### C. Wi-Fi Throughput

The Wi-Fi physical layer protocol has been enhanced during last ten years, including IEEE 802.11 a/g, 802.11n and 802.11ac. According to [14], the current IEEE 802.11 protocol can guarantee a constant maximum throughput for users which are located within 12 m from the transmitter, which is shown in Table. I. In general, the small scale fading in the radio frequency (RF) wireless communication systems results in a fluctuation of the data rates. In order to simplify the analysis complexity, the small scale fading of RF channels is not considered in this study. This assumption is also used in [2] which considers the LB problem in Li-Fi/Wi-Fi network. Therefore here, the distance between users and Wi-Fi AP is set to be within 12 m, and the Wi-Fi throughput is assumed to be constant and equal to the maximum throughput shown in Table. I, which is denoted by $R_0$.

## III. DYNAMIC LOAD BALANCING SCHEME

In this section, a dynamic load balancing scheme for the hybrid Li-Fi/Wi-Fi network is proposed. Firstly, a dynamic algorithm executed by the CU is proposed with the handover overhead taken into consideration. Following that, a load balancing algorithm used in each state is given, including AP assignment and time resource allocation.

**Algorithm 1** Dynamic algorithm executed by the central unit.

```
Initialisation: α'_μ  n ← 1;
while n ≤ N_s do
    for all each μ ∈ U do
        find α' = arg_{α∈C} g^{(n-1)}_{μ,α} = 1;
        for all each α ∈ C do
            Calculate the handover efficiency η_{α'α};
            Calculate r^{(n)}_{μ,α} between μ and α;
        end for
    end for
    Calculate g^{(n)}_{μ,α} and k^{(n)}_{μ,α} based on r^{(n)}_{μ,α} by using load
    balancing algorithm;
    n ← n + 1;
end while
```

### A. Dynamic algorithm executed by the CU

Due to the small coverage area of Li-Fi attocells, the movement of users can probably prompt handover. When the serving AP of a user is switched in two neighbouring states, a handover occurs. In general, the handover overhead in an indoor scenario is in the order of milliseconds, which is assumed to be lower than the state interval $T_p$. According to [8], the overhead time can be modelled as a Poisson random process [15], and the probability mass function (PMF) of the overhead is given by:

$$\Pr(t_{ij} = x) = \frac{\zeta_{ij}^x e^{-\zeta_{ij}}}{x!}, \quad x = 0, 1, 2...(\text{ms}) \tag{6}$$

where $\zeta_{ij} = \mathbb{E}[t_{ij}]$ is the mean of the handover overhead from AP $i$ to AP $j$. The overhead incurs a certain decrease in the average data rate of users that experience handover. In this study, the handover efficiency between two adjacent states is defined as:

$$\eta_{ij} = \begin{cases} \left[1 - \dfrac{t_{ij}}{T_p}\right]^+, & i \neq j \\ 1, & i = j \end{cases}, \qquad i, j \in \mathcal{C}, \tag{7}$$

where $t_{ij}$ is the overhead of AP switch from AP $i$ to AP $j$; and $[.]^+$ is the maximum operator, $\max(\ .\ , 0)$.

The link data rate between AP $\alpha$ and user $\mu$ in state $n$ with handover efficiency can be expressed as:

$$r_{\mu,\alpha}^{(n)} = \begin{cases} \eta_{\alpha'\alpha} R_0, & \alpha = 0 \\ \eta_{\alpha'\alpha} R_{\mu,\alpha}^{(n)}, & \alpha = 1, 2...N_c \end{cases}, \tag{8}$$

where $R_{\mu,\alpha}^{(n)}$ is the Li-Fi data rate according to (5); $\alpha'$ is the AP allocated to user $\mu$ in the state $n-1$; $\eta_{\alpha'\alpha}$ is the handover efficiency from AP $\alpha'$ to AP $\alpha$, according to (7); and $R_0$ is the Wi-Fi throughput.

In each state, the system load balancing, which consists of the AP assignment and communication resource allocation, is undertaken by the CU. Two variables, $g_{\mu,\alpha}^{(n)}$ and $k_{\mu,\alpha}^{(n)}$, are used

to represent the load balancing results in these two aspects respectively. Variable $g_{\mu,\alpha}^{(n)}$ is a binary number which equals 1 when user $\mu$ is served by AP $\alpha$, and equals 0 when $\alpha$ is not the serving AP of this user. Variable $k_{\mu,\alpha}^{(n)}$ is proportion of the resource that user $\mu$ is able to use for communication. The time division multiple access (TDMA) method is applied in each cell, and $k_{\mu,\alpha}^{(n)}$ is considered as the probability that each time resource block is allocated to $\mu$. Thus, $k_{\mu,\alpha}^{(n)}$ is a fractional number between 0 and 1 with $\sum_{\mu} k_{\mu,\alpha}^{(n)} = 1$ for each AP $\alpha$. The number of states considered in this study is denoted by $N_s$. The dynamic algorithm executed by the CU is summarised in Algorithm 1. The load balancing algorithm used in each state is given in Section III-B.

### *B. Load balancing algorithm in each state*

In this section, the load balancing algorithm used in each state is shown, and the superscript $(n)$ is omitted for simplicity. When considering load balancing, it is important to apply an appropriate utility function. In [7], a generalised utility function considering both sum-rate and user fairness is proposed:

$$\gamma_\beta(x) = \begin{cases} \log(x), & \beta = 1 \\ \dfrac{x^{1-\beta}}{1-\beta}, & \beta \geq 0, \beta \neq 1 \end{cases}, \tag{9}$$

where $\beta$ is a proportion coefficient. Specifically, when $\beta = 0$, a linear utility function is realised and the maximal system throughput is achieved; when $\beta = 1$, the proportional fairness is achieved; and when $\beta \to \infty$, the max-min fairness is obtained.

However, according to [16], using a linear utility function for throughput maximisation results in a trivial solution, where each AP serves only its strongest link user. When the utility function for max-min fairness is used, each user achieves the same data rate, but very low sum-throughput. Thus, both are not satisfactory solutions to balance throughput and fairness. In this study, a logarithmic utility function with $\beta = 1$ is used, which achieves proportional fairness [7]. By using the logarithmic utility function, the load balancing problem can be formulated as a utility maximisation problem, which can be expressed as:

$$\max_{g_{\mu,\alpha}, k_{\mu,\alpha}} \quad \sum_{\mu\in\mathcal{U}} \sum_{\alpha=0}^{N_c} g_{\mu,\alpha} \log(k_{\mu,\alpha} r_{\mu,\alpha}) \tag{10}$$

$$\text{s.t.} \quad \sum_{\alpha=0}^{N_c} g_{\mu,\alpha} = 1 \qquad \forall \mu \in \mathcal{U};$$

$$\sum_{\mu\in\mathcal{C}} g_{\mu,\alpha} k_{\mu,\alpha} \leq 1 \qquad \forall \alpha \in \mathcal{C};$$

$$g_{\mu,\alpha} \in \{0,1\}, \quad k_{\mu,\alpha} \in [0,1], \quad \forall \mu \in \mathcal{U}, \forall \alpha \in \mathcal{C};$$

where $r_{\mu,\alpha}$ is the communication link data rate given in (8), which is a positive number. The optimum $k_{\mu,\alpha}$ is shown to be greater than zero in (12) so that $\log(0)$ is avoided.

This is a problem of mixed integer and non-linear programming. A decomposition-based approach can be used to solve the problem by decomposing the original problem into solvable sub-problems according to [17]. Initially, the variable $k_{\mu,\alpha}$ is optimised. With a given $g_{\mu,\alpha}$, the objective function for AP $\alpha$ in (10) can be expressed as:

$$\begin{aligned} F(k_{\mu,\alpha}) &= \sum_{\mu\in\mathcal{U}_\alpha} \log(k_{\mu,\alpha} r_{\mu,\alpha}) \\ &\propto \frac{1}{M_\alpha} \sum_{\mu\in\mathcal{U}_\alpha} \log(k_{\mu,\alpha}) = \log\left[ \left( \prod_{\mu\in\mathcal{U}_\alpha} k_{\mu,\alpha} \right)^{\frac{1}{M_\alpha}} \right] \\ &\leq \log\left( \frac{k_{1,\alpha} + k_{2,\alpha} + ... + k_{M_\alpha,\alpha}}{M_\alpha} \right), \end{aligned} \tag{11}$$

where $\mathcal{U}_\alpha$ is the set of the users allocated to the AP $\alpha$; and $M_\alpha$ represents its cardinality. According to the rule of inequality, the maximum in (11) is achieved only when:

$$k_{\mu,\alpha} = \frac{1}{M_\alpha}, \qquad \forall \mu \in \mathcal{U}_\alpha. \tag{12}$$

According to (12), all of the users allocated to a specific AP share an equal proportion of the time resource. By replacing $k_{\mu,\alpha}$ with $M_\alpha$, the problem in (10) can be re-written as:

$$\max_{g_{\mu,\alpha}, M_\alpha} \quad \sum_{\mu\in\mathcal{U}} \sum_{\alpha=0}^{N_c} g_{\mu,\alpha} \log\left( \frac{r_{\mu,\alpha}}{M_\alpha} \right) \tag{13}$$

$$\text{s.t.} \quad \sum_{\alpha=0}^{N_c} g_{\mu,\alpha} = 1 \qquad \forall \mu \in \mathcal{U}; \tag{14}$$

$$\sum_{\mu\in\mathcal{U}} g_{\mu,\alpha} = M_\alpha \qquad \forall \alpha \in \mathcal{C}; \tag{15}$$

$$g_{\mu,\alpha} \in \{0,1\}, \qquad \forall \mu \in \mathcal{U}, \forall \alpha \in \mathcal{C};$$

The Lagrangian multiplier method is used to solve this problem. The two Lagrangian multipliers $\lambda_\mu$ and $\omega_\alpha$ correspond to the constraints of (14) and (15), respectively. Therefore the Lagrangian function can be expressed as:

$$\begin{aligned} L = &\sum_{\mu\in\mathcal{U}} \sum_{\alpha=0}^{N_c} g_{\mu,\alpha} \log\left( \frac{r_{\mu,\alpha}}{M_\alpha} \right) + \sum_{\mu\in\mathcal{U}} \lambda_\mu \left( 1 - \sum_{\alpha=0}^{N_c} g_{\mu,\alpha} \right) \\ &+ \sum_{\alpha=0}^{N_c} \omega_\alpha \left( M_\alpha - \sum_{\mu\in\mathcal{U}} g_{\mu,\alpha} \right). \end{aligned} \tag{16}$$

Due to $\sum_{\mu\in\mathcal{U}} g_{\mu,\alpha} = M_\alpha$, the Lagrangian function can be re-written as:

$$L = L_1(g_{\mu,\alpha},\ \lambda_\mu, \omega_\alpha) + L_2(M_\alpha, \lambda_\mu, \omega_\alpha), \tag{17}$$

where

$$L_1 = \sum_{\mu\in\mathcal{U}} \sum_{\alpha=0}^{N_c} g_{\mu,\alpha} (\log r_{\mu,\alpha} - \lambda_\mu - \omega_\alpha), \tag{18}$$

$$L_2 = \sum_{\alpha=0}^{N_c} M_\alpha (\omega_\alpha - \log M_\alpha) + \sum_{\mu\in\mathcal{U}} \lambda_\mu. \tag{19}$$

In this case, the problem of (13) can be decomposed into two sub-problems which are to maximise $L_1$ and $L_2$ using the proper Lagrangian multipliers.

Firstly, $\lambda_\mu$ and $\omega_\alpha$ are assumed to be fixed; $L_1$ can be maximised when the following expression is achieved:

$$g^*_{\mu,\alpha} = \begin{cases} 1, \alpha = \arg\max_{\alpha\in\mathcal{C}}(\log r_{\mu,\alpha} - \lambda_\mu - \omega_\alpha) \\ 0, \qquad\qquad \text{otherwise} \end{cases}. \quad (20)$$

Based on (15) and (20), the number of users allocated to AP $\alpha$ can be obtained, which can be written as:

$$M_{\alpha,1} = \sum_{\mu\in\mathcal{U}} g^*_{\mu,\alpha} \quad (21)$$

In addition, given the Lagrangian multipliers, the maximum $L_2$ is obtained when the following expression is achieved:

$$\frac{\partial L_2}{\partial M_\alpha} = 0 \implies M^*_\alpha = \exp(\omega_\alpha - 1). \quad (22)$$

Then, a variable $\delta$ is introduced to represent the difference between $M_{\alpha,1}$ and $M^*_\alpha$, which can be expressed as:

$$\delta = \sum_{\alpha\in\mathcal{C}} |M_{\alpha,1} - M^*_\alpha|. \quad (23)$$

The optimisation problem to maximise the Lagrangian function in (16) is solved iteratively by using the gradient projection method [18], where $\lambda_\mu$ and $\omega_\alpha$ are updated in the opposite direction to the gradient $\nabla L(\lambda_\mu)$ and $\nabla L(\omega_\alpha)$. The $i$-th iteration of the gradient projection algorithm can be expressed as:

$$\lambda_\mu(i+1) = \lambda_\mu(i) - \epsilon_1(1 - \sum_{\alpha\in\mathcal{C}} g^*_{\mu,\alpha}); \quad (24)$$

$$\omega_\alpha(i+1) = \omega_\alpha(i) - \epsilon_2(M^*_\alpha - \sum_{\mu\in\mathcal{U}} g^*_{\mu,\alpha}), \quad (25)$$

where $\epsilon_1$ and $\epsilon_2$ are the sufficiently small step sizes required for guaranteeing convergence. According to (20), $\sum_{\alpha\in\mathcal{C}} g^*_{\mu,\alpha} = 1$ is always satisfied in each iteration, and the expression in (24) is re-written as $\lambda_\mu(i+1) = \lambda_\mu(i)$. Therefore, the Lagrangian multiplier $\lambda_\mu$ can be set to 0, and only $\omega_\alpha$ should be updated in the iteration. An appropriate threshold $\delta_T$ is defined and the variables converge to the optimum when $\delta \le \delta_T$ is achieved. The threshold $\delta_T$ should be small enough but it does not necessarily have to be a particular value. A smaller value of $\delta_T$ will make the convergence slower. The iterative algorithm is shown in Algorithm 2.

**Algorithm 2** : Load balancing algorithm in each state.

Initialisation: $\lambda_\mu(i) = \omega_\alpha(i) = 0$, $i \leftarrow 1$ and $\delta \leftarrow +\infty$;
**while** $\delta \ge \delta_T$ **do**
  **for all** each $\mu \in \mathcal{U}$ **do**
    $\alpha^* = \arg\max_{\alpha\in\mathcal{C}}(\log b_{\mu,\alpha} - \lambda_\mu(i) - \omega_\alpha(i))$;
    $g^*_{\mu,\alpha} = \begin{cases} 1, \alpha = \alpha^* \\ 0, \text{otherwise} \end{cases}$;
  **end for**
  Calculate $M_{\alpha,1} = \sum_{\mu\in\mathcal{U}} g^*_{\mu,\alpha}$, $\forall\alpha \in \mathcal{C}$;
  **for all** each $\alpha \in \mathcal{C}$ **do**
    $M^*_\alpha = \exp(\omega_\alpha(i) - 1)$;
    $\omega_\alpha(i+1) = \omega_\alpha(i) - \epsilon_2(M^*_\alpha - \sum_{\mu\in\mathcal{U}} g^*_{\mu,\alpha})$;
  **end for**
  Calculate $\delta = \sum_{\alpha\in\mathcal{C}} |M_{\alpha,1} - M^*_\alpha|$;
  $i \leftarrow i + 1$;
**end while**
Calculate $g_{\mu,\alpha} = g^*_{\mu,\alpha}$ and $k_{\mu,\alpha} = 1/M^*_\alpha$;

## IV. Analysis of AP Service Area and System Throughput

In order to gain an understanding of the load balancing in a hybrid network, it is important to study the service area of each AP. In this section, the AP service area is identified with a given Wi-Fi throughput, and the throughput of each Li-Fi attocell is analysed. Firstly, a special case without optical CCI is considered, which is termed as the 'Non-CCI' case. Following that, a generic case with CCI is considered, which is termed as the 'Optical CCI' case.

### A. Non-CCI case

In the non-CCI case, users served by Li-Fi APs do not receive any optical signals from other Li-Fi APs. It is assumed that each Li-Fi AP covers the same size of attocell. In order to eliminate the optical interference, the distance between any two Li-Fi APs should be greater than the diameter of Li-Fi attocells.

According to the assumption in Section II-A that the angle of irradiation is equal to the angle of incidence for each user, the following expression can be achieved:

$$\cos(\phi) = \cos(\theta) = \frac{h}{\sqrt{z^2_{\mu,\alpha} + h^2}}, \quad (26)$$

where $z_{\mu,\alpha}$ is the horizontal distance between Li-Fi AP $\alpha$ and user $\mu$; $h$ is the height of the room; $\phi$ is the angle of irradiation; and $\theta$ is the angle of incidence. The channel model in (1) can be expressed as a function with $z_{\mu,\alpha}$, and the data rate between Li-Fi AP $\alpha$ and user $\mu$ can be written as:

$$\rho_\alpha(z_{\mu,\alpha}) = B\log_2(1 + \text{SNR}(z_{\mu,\alpha})) \ge 0, \quad (27)$$

where

$$\text{SNR}(z_{\mu,\alpha}) = \frac{[(m+1)\kappa P_t A_p g(\theta) T_s(\theta) h^{m+1}]^2}{4\pi^2 \iota^2 N_0 B}(z^2_{\mu,\alpha} + h^2)^{-m-3}. \quad (28)$$

It can be seen that $\rho_\alpha(z_{\mu,\alpha})$ is a monotonic decreasing function with respect to $z_{\mu,\alpha}$.

*Lemma 1:* It is assumed that users are optimally allocated to APs by using the proposed load balancing scheme. For any Li-Fi AP $\alpha$, it can be obtained that:

$$z_{i,\alpha} \le z_{j,\alpha}, \qquad \forall i \in \mathcal{U}_\alpha, j \notin \mathcal{U}_\alpha, \quad (29)$$

where $\mathcal{U}_\alpha$ is the set of users allocated to Li-Fi AP $\alpha$.

*Proof:* Firstly, when user $j$ is served by a different Li-Fi AP from AP $\alpha$, this user should reside in the corresponding

Li-Fi attocell. Since the Li-Fi attocells are not overlapped, the inequality $z_{i,\alpha} \leq z_{j,\alpha}$ is satisfied.

When user $j$ is served by the Wi-Fi AP, the method of proof by contradiction is applied to prove this lemma. It is assumed that the optimal load balancing is achieved by using the proposed scheme, and the inequality below is achieved:

$$z_{i,\alpha} > z_{j,\alpha}, \qquad \forall i \in \mathcal{U}_\alpha, j \notin \mathcal{U}_\alpha, \tag{30}$$

where user $i$ is served by Li-Fi AP $\alpha$ and user $j$ is served by the Wi-Fi AP. The objective function in (13) can be written as:

$$\begin{aligned} F_1 =& \log\left(\frac{\rho_\alpha(z_{i,\alpha})}{M_\alpha}\right) + \log\left(\frac{R_0}{M_0}\right) \\ &+ \sum_{\mu \in U-\{i,j\}} \sum_{y=0}^{N_c} g_{\mu,y} \log\left(\frac{\rho_y(z_{\mu,y})}{M_y}\right), \end{aligned} \tag{31}$$

where $M_\alpha$ and $M_0$ are the number of the users served by Li-Fi AP $\alpha$ and the Wi-Fi AP, respectively. Now, the APs allocated to user $i$ and $j$ are exchanged. The values of $M_\alpha$ and $M_0$ stay the same, and the objective function can be re-written as:

$$\begin{aligned} F_2 =& \log\left(\frac{R_0}{M_0}\right) + \log\left(\frac{\rho_\alpha(z_{j,\alpha})}{M_\alpha}\right) \\ &+ \sum_{\mu \in U-\{i,j\}} \sum_{y=0}^{N_c} g_{\mu,y} \log\left(\frac{\rho_y(z_{\mu,y})}{M_y}\right). \end{aligned} \tag{32}$$

Due to the monotonic decrease of $\rho_\alpha(z_{\mu,\alpha})$, it can be obtained that:

$$\rho_\alpha(z_{i,\alpha}) < \rho_\alpha(z_{j,\alpha}). \tag{33}$$

As a consequence, $F_2 > F_1$ is achieved. This means that the AP allocation for user $i$ and $j$ is not optimal, leading to a contradiction. The assumption in (30) must be false and the lemma is proved. ∎

Lemma 1 indicates that users served by Li-Fi AP $\alpha$ are closer to this AP than the users served by other APs. The service area of a Li-Fi AP in the non-CCI case is a circular region, and handover only occurs when users go through the boundary of the circular regions. In this study, the boundary is termed as the 'handover circle', and the centre of the handover circle is the location of a Li-Fi AP. Users that are outside all of the handover circles are served by the Wi-Fi AP.

The radius of the handover circles is analysed as follows. It is assumed that users are uniformly distributed in the entire scenario. The area of the scenario is denoted by $Y$; the density of users is denoted by $\varepsilon$; the radius of the attocell covered by Li-Fi AP $\alpha$ is denoted by $Z_\alpha$; the radius of the handover circle of Li-Fi AP $\alpha$ is denoted by $\nu_\alpha$; and the average handover efficiency is denoted as $\bar{\eta}$, where $\bar{\eta} = \mathbb{E}[\eta_{ij}]$ and $\eta_{ij}$ is given in (7). The number of users served by each AP can be written as:

$$M_\alpha(\nu_\alpha) = \begin{cases} \varepsilon Y - \sum_{\alpha=1}^{\alpha=N_c} \varepsilon\pi\nu_\alpha^2, & \alpha = 0 \\ \sum_{\alpha=1}^{\alpha=N_c} \varepsilon\pi\nu_h^2, & \alpha = 1, 2...N_c \end{cases}, \tag{34}$$

where

$$Y > \sum_{\alpha=1}^{\alpha=N_c} \pi\nu_\alpha^2, \quad 0 < \nu_\alpha \leq Z_\alpha, \tag{35}$$

because all of the Li-Fi attocells are inside the considered scenario. According to the proposed load balancing scheme, the radius of handover circles can be calculated by solving the optimisation problem in (13), which can be written as:

$$\max_{\nu_\alpha} \quad G_1(\nu_\alpha) + G_2(\nu_\alpha) \tag{36}$$

$$s.t. \qquad 0 < \nu_\alpha \leq Z_\alpha \tag{37}$$

where

$$G_1(\nu_\alpha) = \left(\varepsilon Y - \sum_{\alpha=1}^{\alpha=N_c} \varepsilon\pi\nu_\alpha^2\right) \log\left(\frac{\bar{\eta}R_0}{\varepsilon Y - \sum_{\alpha=1}^{\alpha=N_c} \varepsilon\pi\nu_\alpha^2}\right), \tag{38}$$

$$G_2(\nu_\alpha) = 2\pi\varepsilon \sum_{\alpha=1}^{\alpha=N_c} \int_0^{\nu_\alpha} \log\left(\frac{\bar{\eta}\rho_\alpha(x)}{\varepsilon\pi\nu_\alpha^2}\right) x \, \mathrm{d}x. \tag{39}$$

The first order derivatives of $G_1(\nu_\alpha)$ and $G_2(\nu_\alpha)$ can be expressed as:

$$\frac{\partial G_1}{\partial \nu_\alpha} = -2\pi\varepsilon\nu_\alpha \left[\log\left(\frac{\bar{\eta}R_0}{\varepsilon Y - \sum_{\alpha=1}^{\alpha=N_c} \varepsilon\pi\nu_\alpha^2}\right) - 1\right], \tag{40}$$

$$\frac{\partial G_2}{\partial \nu_\alpha} = 2\pi\varepsilon\nu_\alpha \left[\log\left(\frac{\bar{\eta}\rho_\alpha(\nu_\alpha)}{\varepsilon\pi\nu_\alpha^2}\right) - 1\right]. \tag{41}$$

The derivative of the objective function in (36) can therefore be expressed as:

$$\frac{\partial(G_1 + G_2)}{\partial \nu_\alpha} = 2\pi\varepsilon\nu_\alpha \log\left(\frac{\rho_\alpha(\nu_\alpha)(Y - \sum_{\alpha=1}^{\alpha=N_c} \pi\nu_\alpha^2)}{\pi\nu_\alpha^2 R_0}\right). \tag{42}$$

Due to $\nu_\alpha > 0$, $\frac{\partial(G_1+G_2)}{\partial \nu_\alpha}$ can be equal to 0 only when

$$\hat{\nu}_\alpha = F^{-1}(1) > 0, \tag{43}$$

where $F^{-1}$ is the inverse function of $F(\nu_\alpha)$, which is

$$F(\nu_\alpha) = \frac{\rho_\alpha(\nu_\alpha)(Y - \sum_{\alpha=1}^{\alpha=N_c} \pi\nu_\alpha^2)}{\pi\nu_\alpha^2 R_0}, \tag{44}$$

where $F(\nu_\alpha) > 0$ with $0 < \nu_\alpha \leq Z_\alpha$ due to the conditions in (27) and (35). It can be seen that the function $F(\nu_\alpha)$ is monotonic decreasing with respect to $\nu_\alpha$.

When $0 < \hat{\nu}_\alpha \leq Z_\alpha$ is satisfied, it can be obtained that:

$$\left.\frac{\partial^2(G_1 + G_2)}{\partial \nu_\alpha^2}\right|_{\nu_\alpha = \hat{\nu}_\alpha} \tag{45}$$

$$= 2\pi\varepsilon \left[\log(F(\hat{\nu}_\alpha)) + \frac{\hat{\nu}_\alpha}{F(\hat{\nu}_\alpha)} \left.\frac{\partial F(\nu_\alpha)}{\partial \nu_\alpha}\right|_{\nu_\alpha = \hat{\nu}_\alpha}\right] < 0, \tag{46}$$

where $\frac{\partial F(\nu_\alpha)}{\partial \nu_\alpha} < 0$ due to monotonic decrease property. As a consequence, $\hat{\nu}_\alpha$ is the optimum for the problem in (36). When $\hat{\nu}_\alpha > Z_\alpha$, since $F(\nu_\alpha)$ is monotonically decreasing, the optimum $\nu_\alpha$ equals to $Z_\alpha$. The radius of handover circles can be expressed as:

$$\nu_\alpha^* = \begin{cases} Z_\alpha, & \hat{\nu}_\alpha > Z_\alpha \\ \hat{\nu}_\alpha, & \hat{\nu}_\alpha \leq Z_\alpha \end{cases}. \tag{47}$$

The sum throughput achieved by AP $\alpha$ can be written as:

$$R_{\text{sum},\alpha} = \begin{cases} R_0, & \alpha = 0; \\ \frac{2}{(\nu_\alpha^*)^2} \int_0^{\nu_\alpha^*} \rho_\alpha(x) x \, \mathrm{d}x, & \alpha = 1, 2...N_c \end{cases}. \tag{48}$$

According to (27) and (44), the Li-Fi APs with the same transmit power and modulation bandwidth have the same radius of the handover circles and throughput.

Since all of the users served by an AP share the equal time resource, the resource proportion can be expressed as:

$$k_{\mu,\alpha} = \begin{cases} \frac{1}{\varepsilon(Y-\sum_{\alpha=1}^{\alpha=N_c}\pi(\nu_\alpha^*)^2)}, & \alpha = 0; \\ \frac{1}{\varepsilon\pi(\nu_\alpha^*)^2}, & \alpha = 1,2...N_c \end{cases}. \tag{49}$$

According to (44) and (47), it can be obtained that:

$$F(\nu_\alpha^*) \geq 1 \tag{50}$$

$$\Longleftrightarrow \quad \frac{\rho_\alpha(\nu_\alpha^*)}{\varepsilon\pi(\nu_\alpha^*)^2} \geq \frac{R_0}{\varepsilon(Y-\sum_{\alpha=1}^{\alpha=N_c}\pi(\nu_\alpha^*)^2)} \tag{51}$$

$$\Longleftrightarrow \quad \frac{\rho_\alpha(\nu_\alpha^*)}{k_{\mu,\alpha}} \geq \frac{R_0}{k_{\mu,0}}, \quad \alpha = 1,2...N_c \tag{52}$$

where the equality in (52) is achieved when $\hat{\nu_\alpha} \leq Z_\alpha$. This inequality indicates that the users served by Li-Fi APs achieve data rates higher than or equal to those served by the Wi-Fi AP.

In addition, since $\rho_\alpha(\nu_\alpha)$ is monotonically decreasing, the Li-Fi throughput increases with a reduction of the radius of handover circles. According to (44), an increase of Wi-Fi throughput results in a decrease of $\nu_\alpha^*$, thus leading to an improvement of Li-Fi throughput. This means that the Wi-Fi throughput has a significant effect on the Li-Fi throughput in the hybrid network even though they work on different ranges of electromagnetic spectrum.

### *B. Optical CCI case*

In this case, the Li-Fi attocells overlap with each other, and the optical CCI is considered. When Li-Fi APs are positioned very closely, the achievable spectral efficiency in the Li-Fi systems would be significantly affected by the CCI. In order to avoid high level of CCI, the distance between Li-Fi APs is set to be greater than the radius of an attocell. In the case that the distance is less than or equal to the radius, the technology fractional frequency reuse (FFR) [19] and spatial division multiple access (SDMA) [20] can be used to mitigate the strong interference, which is outside the scope of this study and is not discussed here.

According to Lemma 1, users served by Li-Fi APs must reside in the handover circles. Thus, when a handover circle does not overlap with other attocells, users allocated to the corresponding Li-Fi AP do not experience optical CCI, as shown in Fig. 2(a). In this case, the condition (29) in Lemma 1 is satisfied in this Li-Fi attocell. However, when a handover circle overlaps with other Li-Fi attocells, shown in Fig. 2(b), some of the users served by this Li-Fi AP would be affected by optical CCI.

In the case of optical CCI, the communication link data rate between Li-Fi AP $\alpha$ and user $\mu$ can be expressed as:

$$\rho_\alpha(\text{SINR}_{\mu,\alpha}) = B\log_2(1+\text{SINR}(z_{\mu,\alpha})), \tag{53}$$

where $\text{SINR}_{\mu,\alpha}$ is given in (4). In general, when a user experiences interference from more than one Li-Fi AP, the achievable SINR performance would be less than 0 dB, as shown in [21]. In this case, the Li-Fi link data rate is much lower than that of Wi-Fi. Accordingly, users in such multi-overlap areas are assumed to have no Li-Fi access, and this paper mainly focuses on the load balancing analysis for the overlap areas of two Li-Fi attocells.

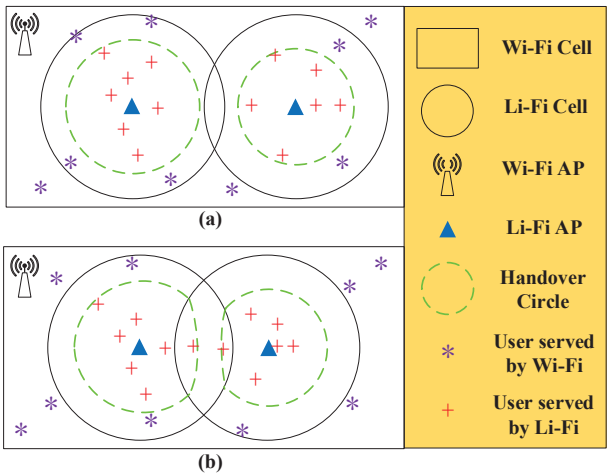


Fig. 2. Handover Circle Illustration

*Lemma 2:* For each Li-Fi AP $\alpha$,

$$\text{SINR}_{i,\alpha} \geq \text{SINR}_{j,\alpha}, \qquad \forall i \in \mathcal{U}_\alpha, j \notin \mathcal{U}_\alpha, \tag{54}$$

where $\mathcal{U}_\alpha$ is the set of users allocated to Li-Fi AP $\alpha$.

*Proof:* Initially, if $j$ is allocated to the Wi-Fi AP, this lemma is proved by using the method shown in the proof of Lemma 1.

Then, the case that user $j$ is served by another Li-Fi AP $\alpha'$ is considered, and the method of proof by contradiction is applied to prove this lemma. It is assumed that:

$$\text{SINR}_{i,\alpha} < \text{SINR}_{j,\alpha}, \qquad \forall i \in \mathcal{U}_\alpha, j \in \mathcal{U}_{\alpha'}, \tag{55}$$

where $\mathcal{U}_{\alpha'}$ is the set of the users allocated to Li-Fi AP $\alpha'$. According to the assumption in (55), the expression $\text{SINR}_{j,\alpha'} < \text{SINR}_{i,\alpha'}$ is achieved. Particularly, if user $i$ or $j$ is outside the overlap area and cannot served by one of the APs between $\alpha$ and $\alpha'$, the corresponding SINR is 0.

The objective function in (13) can be written as:

$$F_3 = \log\left(\frac{\rho_\alpha(\text{SINR}_{i,\alpha})}{M_\alpha}\right) + \log\left(\frac{\rho_\alpha(\text{SINR}_{j,\alpha'})}{M_{\alpha'}}\right) + \sum_{\mu\in\mathcal{U}-\{i,j\}}\sum_{y=0}^{N_c} g_{\mu,y}\log\left(\frac{\rho_y(\text{SINR}_{\mu,y})}{M_y}\right), \tag{56}$$

where $M_\alpha$ and $M_{\alpha'}$ represent the number of users served by Li-Fi AP $\alpha$ and $\alpha'$, respectively.

Now, the allocated APs of user $i$ and $j$ are exchanged. The values of $M_\alpha$ and $M_{\alpha'}$ stay the same. In this way, the objective function can be written as:

$$F_4 = \log\left(\frac{\rho_\alpha(\text{SINR}_{j,\alpha})}{M_\alpha}\right) + \log\left(\frac{\rho_\alpha(\text{SINR}_{i,\alpha'})}{M_{\alpha'}}\right) + \sum_{\mu\in\mathcal{U}-\{i,j\}}\sum_{y=0}^{N_c} g_{\mu,y}\log\left(\frac{\rho_y(\text{SINR}_{\mu,y}}{M_y}\right). \tag{57}$$

According to (55), it can be derived that $F_4 > F_3$. This means that the allocation of APs for these two users in this assumption is not optimal, leading to a contradiction. Consequently, the assumption in the proof must be false so that this lemma is proved.

■

According to Lemma 2, all of the users served by a Li-Fi AP achieve higher SINR than that of other users. The distribution of $\text{SINR}_{\mu,\alpha}$ is closely related to the distance between the user and the serving AP, and between the user and the interfering AP. In general, a high $\text{SINR}_{\mu,\alpha}$ is achieved when a user is close to the serving AP and far away from the interference AP. The boundary of the service area of Li-Fi APs is shown in Fig. 2(b). However, the specific shape of the Li-Fi service area in the optical CCI case is significantly affected by the layout of the Li-Fi APs. The analysis of the deployment optimisation of Li-Fi APs is outside the scope of this study. Hence the numerical estimation is used to analyse the service areas of Li-Fi APs and the Li-Fi system throughput, and this is given in Section V.

### C. Limitation of the Wi-Fi model

In the practical scenario, the Wi-Fi throughput cannot be uniformly distributed in space due to small scale fading. In this hybrid network, due to the fluctuating CSI of moving users, the network load balancing procedure is undertaken in each state. If the coherence time of the channel in Wi-Fi is larger than the duration of the state, the system would be stable. Otherwise, the average CSI of users in each state can be used for load balancing in order to guarantee the stability of the system. Therefore, in each state, users would achieve different Wi-Fi throughputs $R_0$ in (8) based on their CSI, and the proposed load balancing scheme can still be effective in this practical scenario. In fact, the data rate performance in both Li-Fi and Wi-Fi stand-alone network fluctuates in space. By using the proposed scheme, each user is allocated to a better AP between the best Li-Fi AP and the Wi-Fi AP in terms of data rates, and thus the hybrid network can achieve the diversity gain of two-tier networks. When the Wi-Fi throughput is constant, users inside the handover circles are served by Li-Fi APs. This is because Li-Fi offers higher data rate for these users than Wi-Fi. When considering the spatial fluctuation of Wi-Fi throughput, the boundary of the handover circle would be irregularly fluctuating instead of strictly circular shape. Also, if some users inside the handover circles achieve better CSI with Wi-Fi than with Li-Fi, they would be allocated to the Wi-Fi AP. Therefore, the serving area of Li-Fi APs cannot be a connected region in the practical Li-Fi/Wi-Fi hybrid network. In this study, in order to reduce the analysis complexity of the system throughput, a constant Wi-Fi throughput in space is considered. In future research, the load balancing problem with a more practical Wi-Fi model will be studied.

## V. Performance Evaluation

### A. Simulation setup

In the simulation, the hybrid network constituted by a Wi-Fi AP and four Li-Fi APs is considered. The radius of each Li-Fi attocell is 4 m, and all of the optical attocells reuse the same modulation bandwidth. According to the analysis in Section IV, two different Li-Fi AP deployments are considered in the simulation, the non-CCI case and the optical CCI case. In the non-CCI case, the size of the indoor scenario is 16 m $\times$ 16 m, shown in Fig. 3 (Case 1). The distance between any two neighbouring Li-Fi APs is 8 m and there is no optical CCI. In optical CCI case, the size of the indoor scenario is 13.6 m $\times$ 13.6 m, shown in Fig. 3 (Case 2). The distance between any two neighbouring Li-Fi APs is 5.6 m, and users in the overlapping areas experience optical CCI. The user density is set to be 0.2 person/m$^2$ in these two scenarios, which follows the normal user density in indoor office scenarios. Users are uniformly distributed and moving randomly in the considered scenario, and the random way point model is applied [22]. Specifically, each user selects a random destination in the scenario and moves towards the destination with a random speed between 0 and 1 metre per second. After reaching the destination, a new destination is selected and the user keeps moving. The average handover efficiency is defined as $\eta = \mathbb{E}[\eta_{ij}]$, where $\eta_{ij}$ is according to (7). The Wi-Fi throughput used in the simulation is based on Table. I. The other parameters are summarised in Table II, which are based on the published research [2], [21], [23].

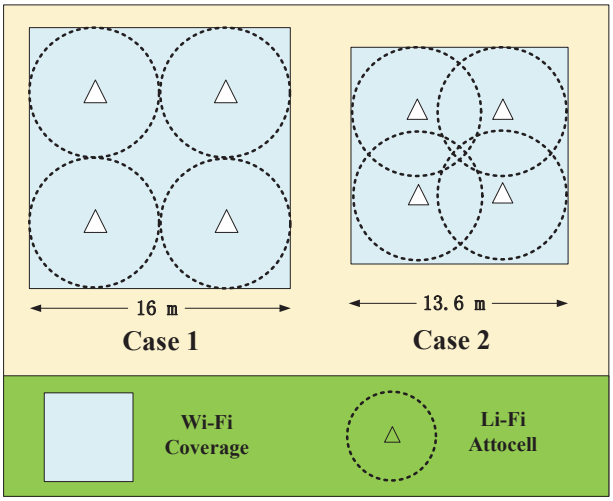


Fig. 3. Simulation Scenario

TABLE II
Simulation Parameters

| Name of Parameters | Value |
|---|---|
| Radius of a Li-Fi cell | 4 m |
| Height of the room | 2.3 m |
| Electric power to optical power conversion, $\iota$ | 3 |
| Transmit optical power per Li-Fi AP, $P_t$ | 10 W |
| Baseband bandwidth for LED lamp, $B$ | 20 MHz |
| Physical area of a PD, $A_p$ | 1 cm$^2$ |
| Half-intensity radiation angle, $\theta_{1/2}$ | 60 deg. |
| Gain of optical filter, $T_s(\theta)$ | 1.0 |
| Receiver FoV semi-angle, $\Theta_F$ | 60 deg. |
| Refractive index, $\chi$ | 1.5 |
| Optical to electric conversion efficiency, $\gamma$ | 0.53 A/W |
| Noise power spectral density, $N_0$ | $10^{-19}$ $A^2$/Hz |
| Resource allocation interval of central unit, $T_p$ | 500 ms |

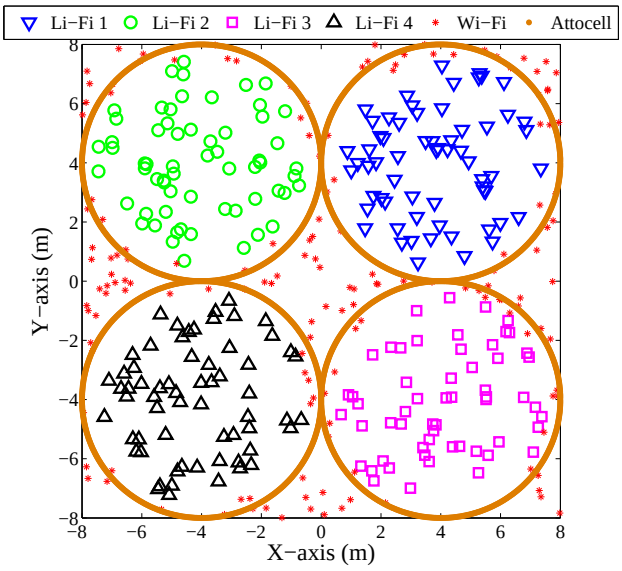


Fig. 4. Simulated location of users served by different AP in non-CCI case. (Wi-Fi sum-throughput 120 Mb/s)

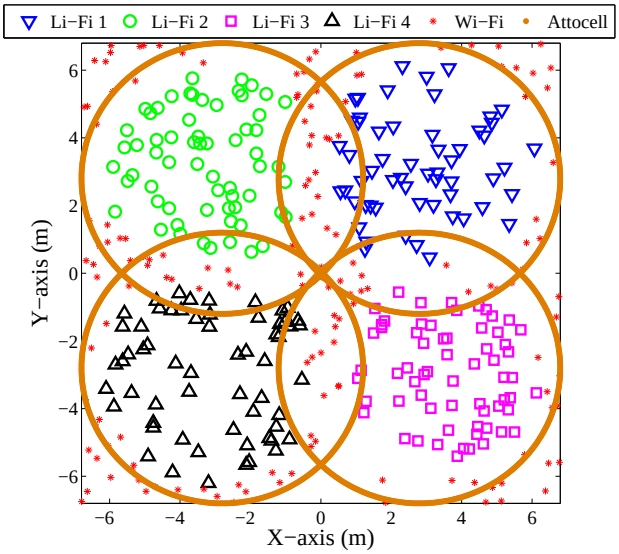


Fig. 6. Simulated location of users served by different AP in optical CCI case. (Wi-Fi sum-throughput 120 Mb/s)

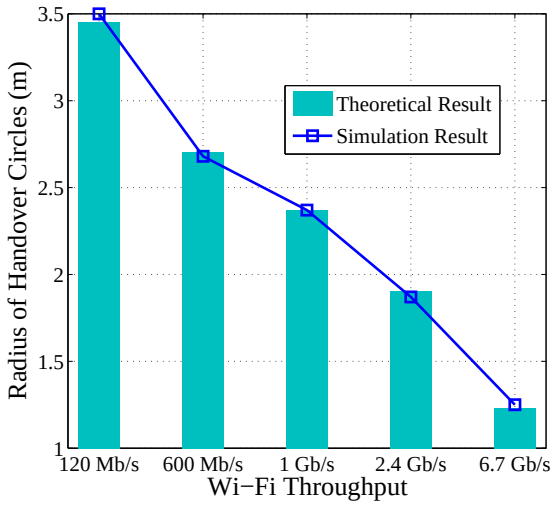


Fig. 5. The analysed and simulated radius of handover circles in non-CCI case.

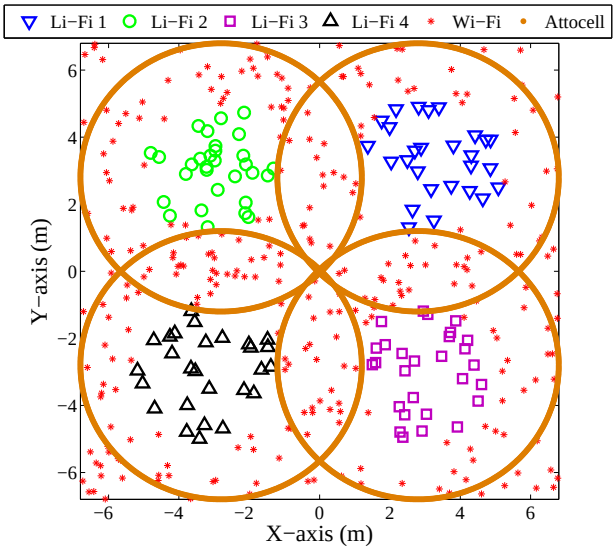


Fig. 7. Simulated location of users served by different AP in optical CCI case. (Wi-Fi sum-throughput 1 Gb/s)

### *B. Study of Li-Fi service areas*

In order to study the Li-Fi service area, a static system is considered where all of the users are fixed. In the non-CCI case, according to the analysis in Section IV-A, users served by a Li-Fi AP must reside in the corresponding handover circle. As shown in Fig. 4, users served by 4 Li-Fi APs and the Wi-Fi AP are marked with different signs. There are clear boundaries between the service areas of different APs, and all of the users served by Li-Fi APs are located inside the region with a circular shape. Since each Li-Fi AP uses the same configuration for wireless communications, their handover circles have the same radius.

In Fig. 5, the simulated and theoretical results of the radius of handover circle are shown. It can be seen that the simulation results match the theoretical results very well. When the Wi-Fi throughput increases, the radius of the handover region decreases because the Wi-Fi AP provides a larger capacity to serve more users. Since the users closer to Li-Fi APs can achieve higher data rates, the sum-throughput of Li-Fi increases when the Li-Fi serving area decreases.

In the optical CCI case, the service areas of the 4 Li-Fi APs and the Wi-Fi AP with optical CCI is shown in Fig. 6 and Fig. 7, and the Wi-Fi throughputs are 120 Mb/s and 1 Gb/s, respectively. It can be seen that the service area of each Li-Fi AP is a connected region but does not have a circular shape. Similar to the non-CCI case, the serving areas of Li-Fi APs decrease with an increase of Wi-Fi throughput. Due to optical CCI, users in the overlap area of Li-Fi attocells are more likely to select the Wi-Fi AP when the Wi-Fi throughput increases. As shown in Fig. 7, all of the users in the overlap area are

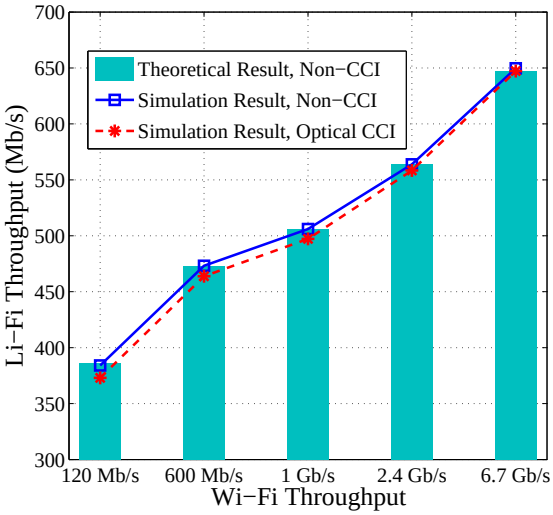


Fig. 8. Evaluation of Li-Fi throughput with different setup of Wi-Fi throughputs in non-CCI and optical CCI cases. ($\eta = 1$)

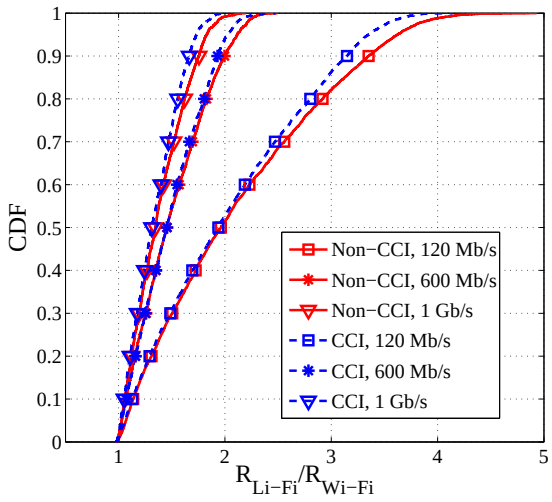


Fig. 9. CDF of the user data ratio $R_{\text{Li-Fi}}/R_{\text{Wi-Fi}}$ in non-CCI and optical CCI case. The user density is set to be 0.2 person/m$^2$, which is normal in the indoor office scenario. ($\eta = 1$)

served by Wi-Fi when Wi-Fi throughput reaches 1 Gb/s.

### C. Study of user data rates

In Fig. 8, the relationship between the Li-Fi throughput and the Wi-Fi throughput is shown. In the non-CCI case, the theoretical Li-Fi throughput corresponding to the Wi-Fi throughput is evaluated, which matches the simulation results very well. In the optical CCI case, the performance of Li-Fi throughput is lower than that of the non-CCI case. The difference decreases with an increase of Wi-Fi throughput. This is because in the optical CCI case the overlap area between the serving region of each Li-Fi AP and the attocells of other interfering Li-Fi APs becomes smaller when the Wi-Fi throughput increases. Thus, the optical CCI case tends to the non-CCI case if Wi-Fi throughput is large enough.

The data rate performance of each user is evaluated and shown in Fig. 9. According to the analysis in Section III-B, all of the users served by a specific AP share an equal time resource. Thus users served by the Wi-Fi AP achieve an equal data rate due to the spatially uniform distribution of Wi-Fi throughput. The data rate ratio $R_{\text{Li-Fi}}/R_{\text{Wi-Fi}}$ is used to evaluate the data rate performance of users, where $R_{\text{Li-Fi}}$ represents the data rate of users served by Li-Fi APs, and $R_{\text{Wi-Fi}}$ is the data rate of users served by the Wi-Fi AP. It is shown that the ratio in both non-CCI and optical CCI case is larger than 1. This indicates that users served by Li-Fi APs always achieve higher data rates than those served by the Wi-Fi AP, which means that the Li-Fi APs can offer a very good quality of service in the hybrid network. The range of the ratio decreases with an increase of Wi-Fi throughput in both the non-CCI and the optical CCI case. Also, the non-CCI case outperforms the optical CCI case with different Wi-Fi throughputs because of the effect of interference.

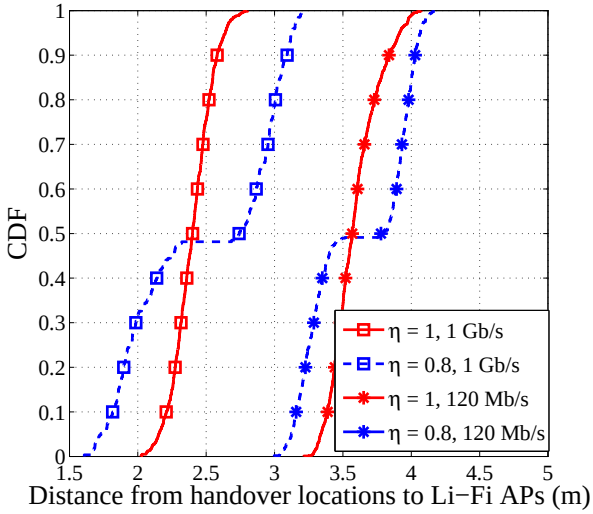


Fig. 10. CDF of the distance between the Li-Fi APs and the handover location in non-CCI case.

### D. Study of handover locations

In this subsection, the handover location of moving users in the hybrid network is studied. In the non-CCI case, the handover occurs only between a Li-Fi AP and the Wi-Fi AP. The distance between the handover location and the Li-Fi AP is used to represent the handover location information. In the optical CCI case, as well as the handover between Li-Fi and Wi-Fi, handover also occurs between two Li-Fi APs. In this situation, the distance between the handover location and the previous serving Li-Fi AP is used for evaluation.

The CDF of the distance which represents the handover location information in the non-CCI case is given in Fig. 10. An interesting result is that when $\eta < 1$, the values of the distance are mainly in two different ranges. This is because the handover overhead results in a handover location offset from the handover circles. For example, if there is no handover

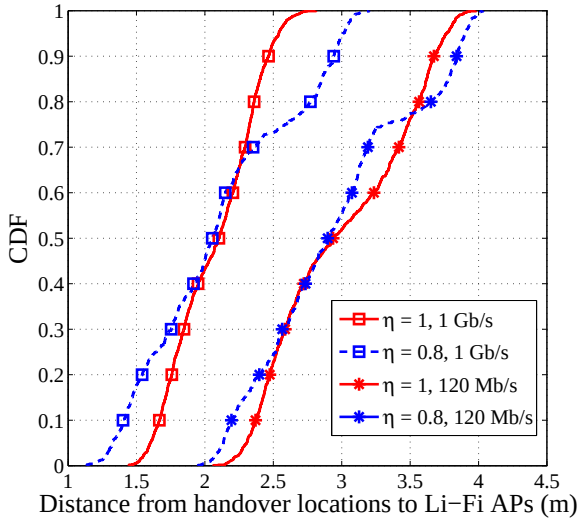


Fig. 11. CDF of the distance between the Li-Fi APs and the handover location in optical CCI case.

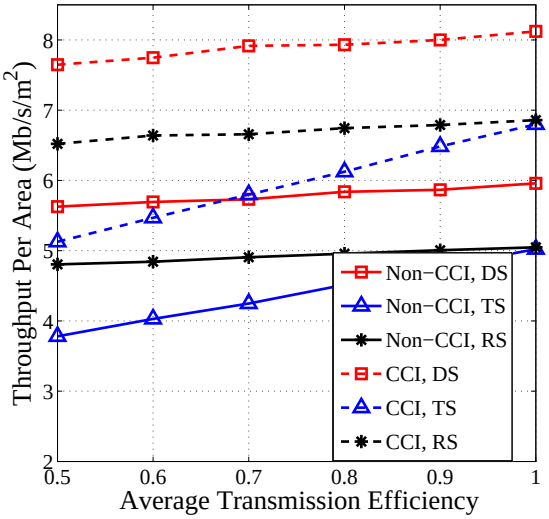


Fig. 12. Spatial throughput in non-CCI case and optical CCI case. ( Wi-Fi throughput 1 Gb/s)

overhead, the handover from Li-Fi to Wi-Fi occurs immediately when users move outside the handover circles. However, with $\eta < 1$, the Wi-Fi data rate is not high enough to prompt a handover due to the loss caused by potential handover. Hence, the handover does not occur on the boundary of handover circles. When users move further away from the Li-Fi AP, the decrease of Li-Fi data rates finally results in handover. Due to the handover overhead, the distance of handover from a Li-Fi AP to the Wi-Fi AP is larger than the radius of handover circle. Similarly, when the handover is from the Wi-Fi AP to a Li-Fi AP, the distance is less than the radius of handover circles. In addition, a smaller handover efficiency leads to a larger offset. The simulation results also indicate that when the Wi-Fi throughput increases, the handover location becomes closer to the Li-Fi AP. This is because the radius of handover circle decreases.

In the optical CCI case, a handover can occur in both non-overlap areas and overlap areas between Li-Fi attocells. As shown in Fig. 11, the values of the distance are still mainly in two different ranges with $\eta < 1$, but around 70% of these values lie in the lower range. This is because the Li-Fi serving regions in the optical CCI case are in an irregular shape, and the Li-Fi AP is closer to the boundary of service regions in the overlap area than that in the non-overlap area. Also, similar to the non-CCI case, the distance between handover locations and Li-Fi APs decreases with an increase of the Wi-Fi throughput.

### *E. Proposed scheme vs. other load balancing schemes*

In this subsection, the system throughput of a hybrid Li-Fi/Wi-Fi network is studied. In order to fairly compare the non-CCI case and the optical CCI case, the spatial throughput (throughput per area) is used for evaluation, and is defined as:

$$\text{Spatial Throughput} = \frac{\text{System Throughput}}{\text{Area of Indoor Scenario}}. \quad (58)$$

The spatial throughput reflects the performance of user data rate with a given user density, which can be expressed as:

$$\text{Average user data rate} = \frac{\text{Spatial Throughput}}{\text{User density}}. \quad (59)$$

The spatial throughputs in both the non-CCI and the optical CCI cases are evaluated and shown in Fig. 12. In the legend, the proposed dynamic load balancing scheme is termed as 'DS', and two other load balancing schemes are considered, termed as 'TS' and 'RS' respectively. In 'TS', a threshold is used to determine whether a user is allocated to the best Li-Fi AP or the Wi-Fi AP [23]. In 'RS', users randomly select the AP between the best Li-Fi AP and the Wi-Fi AP. In both schemes, users served by the same AP share an equal proportion of time resource, and the handover overhead is considered. As shown in Fig. 12, the spatial throughput in the optical CCI case is higher than that of the non-CCI case. This indicates that with the same user density, each user in the optical CCI case can achieve higher data rate despite the interference, resulting from the highly reuse of the communication bandwidth. The spatial throughput decreases with the handover efficiency due to the effect of overhead. The proposed load balancing scheme always outperforms 'TS' and 'RS' with any value of $\eta$. The difference is more than 1 Mb/s/m$^2$. This is because the AP assignment and time resource allocation in 'DS' are jointly designed, which are formulated as an optimisation problem shown in (10), while they are separately designed in 'TS' and 'RS', which are undertaken in sequence [23].

In addition to the indoor Li-Fi/Wi-Fi scenario, the proposed dynamic load balancing scheme can also be used in hybrid RF small cell networks which combine femto-cells and pico-cells [24]. The pico-cells have a very small coverage which is close to Li-Fi attocells (e.g. 60 GHz mmWave). Therefore, handover occurs frequently in these scenarios, and the proposed scheme can offer an efficient and stable load balancing

for the femto/pico hybrid networks.

## VI. Conclusion

In this study, a dynamic load balancing scheme in a Li-Fi/Wi-Fi hybrid network is proposed, where the handover overhead is considered. By analysing the service areas of the Li-Fi APs, the throughput performance of the hybrid system is theoretically studied. Also, the effects of the handover overhead on handover locations and user throughput are simulated and discussed. Three conclusions are made based on the analytical and simulation results: i) the service coverage of Li-Fi APs are connected regions, which are generally smaller than the entire Li-Fi attocells. Specifically, these areas are circular in the non-CCI case, but non-circular in the optical CCI case; ii) the Wi-Fi and Li-Fi throughputs in the hybrid network are related despite the independent spectrum transmission. The Li-Fi throughput can be improved by increasing the Wi-Fi throughput. In addition, the achievable data rates of the users served by Li-Fi APs are higher than or equal to that of users allocated to the Wi-Fi AP; iii) a handover occurs only when users move across the boundaries of the Li-Fi service areas. The handover overhead can lead to a handover location offset due to the transmission loss considered in the proposed load balancing scheme.

## References


[1] D. Tsonev, S. Videv, and H. Haas, "Light Fidelity (Li-Fi): Towards All-optical Networking," Dec. 2013.

[2] X. Li, R. Zhang, and L. Hanzo, "Cooperative Load Balancing in Hybrid Visible Light Communications and WiFi," *IEEE Transactions on Communications*, vol. 63, no. 4, pp. 1319–1329, April 2015.

[3] M. Rahaim, A. Vegni, and T. Little, "A Hybrid Radio Frequency and Broadcast Visible Light Communication System," *IEEE GLOBECOM Workshops 2011*, pp. 792–796, Dec. 2011.

[4] C. Hansen, "WiGig: Multi-gigabit wireless communications in the 60 ghz band," *Wireless Communications, IEEE*, vol. 18, no. 6, pp. 6–7, December 2011.

[5] D. Tsonev, C. Hyunchae, and S. Rajbhandari, "A 3-Gb/s Single-LED OFDM-Based Wireless VLC Link Using a Gallium Nitride uLED," *IEEE Photonics Technology Letters*, vol. 26, pp. 637–640, 2014.

[6] I. Stefan, H. Burchardt, and H. Haas, "Area Spectral Efficiency Performance Comparison between VLC and RF Femtocell Networks," in *Communications (ICC), 2013 IEEE International Conference on*, June 2013, pp. 3825–3829.

[7] F. Jin, R. Zhang, and L. Hanzo, "Resource Allocation under Delay-Guarantee Constraints for Heterogeneous Visible-Light and RF Femtocells," *Wireless Communications, IEEE Transactions on*, vol. PP, no. 99, pp. 1–1, 2014.

[8] M. Kassab, M. Bonnin, and A. Belghith, "Fast and Secure Handover in WLANs: An Evaluation of the Signaling Overhead ," *CCNC*, pp. 770–775, 2008.

[9] M. Vegni and C. Little, "Handover in VLC Systems with Cooperating Mobile Devices ," *CCNC*, pp. 126–130, 2012.

[10] H. Choi, "An Optimal Handover Decision for Throughput Enhancement," *IEEE Comm. Letters*, vol. 14, no. 2, pp. 851–853, 2010.

[11] J. Kahn and J. Barry, "Wireless Infrared Communications," *Proc. IEEE*, vol. 85, no. 2, pp. 265–298, Feb. 1997.

[12] V. Jungnickel, V. Pohl, S. Nonnig, and C. von Helmolt, "A physical model of the wireless infrared communication channel," *Selected Areas in Communications, IEEE Journal on*, vol. 20, no. 3, pp. 631–640, Apr 2002.

[13] S. Dimitrov and H. Haas, "Optimum Signal Shaping in OFDM-Based Optical Wireless Communication Systems," in *Vehicular Technology Conference (VTC Fall), 2012 IEEE*, Sept 2012, pp. 1–5.

[14] E. Perahia and R. Stacey, "Next Generation Wireless LAN: 802.11n and 802.11ac ," *Cambridge University Press*, 2013.

[15] Y. Zhou, A. Pahwa, and S.-S. Yang, "Modeling weather-related failures of overhead distribution lines," *Power Systems, IEEE Transactions on*, vol. 21, no. 4, pp. 1683–1690, Nov 2006.

[16] Q. Ye, B. Rong, Y. Chen, M. Al-Shalash, C. Caramanis, and J. Andrews, "User association for load balancing in heterogeneous cellular networks," *Wireless Communications, IEEE Transactions on*, vol. 12, no. 6, pp. 2706–2716, June 2013.

[17] S. Boyd and L. Vandenberghe, "Convex Optimization," *Cambridge University Press*, 2004.

[18] D. Bertsekas and J. Tsitsiklis, "Parallel and Distributed Computation:Numerical Methods," *Prentice-Hall, Inc.*, 1989.

[19] C. CHEN, S. Videv, D. Tsonev, and H. Haas, "Fractional Frequency Reuse in DCO-OFDM-based Optical Attocell Networks," *Lightwave Technology, Journal of*, vol. PP, no. 99, pp. 1–1, 2015.

[20] Z. Rong and S. Gray, "Beamforming Loss due to Tracking Error in Downlink SDMA," in *Universal Personal Communications, 1998. ICUPC '98. IEEE 1998 International Conference on*, vol. 1, Oct 1998, pp. 441–444 vol.1.

[21] M. Chen, C. Ijaz, D. Tsonev, and H. Haas, "Analysis of Downlink Transmission in DCO-OFDM-Based Optical Attocell Networks," in *Global Communications Conference Exhibition and Industry Forum, 2014 IEEE*, Dec. 2014.

[22] C. Tsao, Y.-T. Wu, W. Liao, and J.-C. Kuo, "Link duration of the random way point model in mobile ad hoc networks," in *IEEE WCNC*, vol. 1, April 2006, pp. 367–371.

[23] D. A. Basnayaka and H. Haas, "Hybrid RF and VLC systems: Improving user data rate performance of VLC system," *IEEE Vehicular Technology Conference (VTC Spring)*, May 2014.

[24] A. Kamal and V. Mathai, "A Novel Cell Selection Method for LTE HetNet," in *2014 International Conference on Communications and Signal Processing (ICCSP)*, April 2014, pp. 738–742.



**Yunlu Wang** received the B.Eng. degree in Telecommunication Engineering in 2011 from the Beijing University of Post and Telecommunications, China, and the double M.Sc. degrees in Digital Communication and Signal Processing in 2013 from the University of Edinburgh, UK, and in Electronic and Electrical Engineering in 2014 from Beihang University, China, respectively. Currently, he is pursuing a Ph.D. degree in Electrical Engineering at the University of Edinburgh. His research focus is on visible light communication (VLC) and radio frequency (RF) hybrid networking.

**Harald Haas** (S'98-AM'00-M'03) received the Ph.D. degree from the University of Edinburgh in 2001. He currently holds the Chair of Mobile Communications at the University of Edinburgh. His main research interests are in optical wireless communications, hybrid optical wireless and RF communications, spatial modulation, and interference coordination in wireless networks. He first introduced and coined spatial modulation and Li-Fi. Li-Fi was listed among the 50 best inventions in TIME Magazine 2011. Prof. Haas was an invited speaker at TED Global 2011, and his talk has been watched online more than 1.5 million times. He is co-founder and chief scientific officer of pureLiFi Ltd. Prof. Haas holds 31 patents and has more than 30 pending patent applications. He has published 300 conference and journal papers including a paper in Science. He was co-recipient of a best paper award at the IEEE Vehicular Technology Conference in Las Vegas in 2013 and in Glasgow in 2015. In 2012, he was the only recipient of the prestigious Established Career Fellowship from the EPSRC (Engineering and Physical Sciences Research Council) within Information and Communications Technology in the UK. Prof. Haas is recipient of the Tam Dalyell Prize 2013 awarded by the University of Edinburgh for excellence in engaging the public with science. In 2014, he was selected by EPSRC as one of ten RISE (Recognising Inspirational Scientists and Engineers) Leaders.